Three-Dimensional Simulations of the Electrothermal and Terahertz Emission Properties of $Bi_2Sr_2CaCu_2O_8$ Intrinsic Josephson Junction Stacks

F. Rudau,[1] R. Wieland,[1] J. Langer,[1] X. J. Zhou,[2,3] M. Ji,[2,3] N. Kinev,[4] L. Y. Hao,[2,3] Y. Huang,[2,3] J. Li,[3] P. H. Wu,[3] T. Hatano,[2] V. P. Koshelets,[4] H. B. Wang,[2,3] D. Koelle,[1] and R. Kleiner[1]

[1]*Physikalisches Institut and Center for Quantum Science (CQ) in LISA+, Universität Tübingen, D-72076 Tübingen, Germany*

[2]*National Institute for Materials Science, Tsukuba 3050047, Japan*

[3]*Research Institute of Superconductor Electronics, Nanjing University, Nanjing 210093, China*

[4]*Kotel'nikov Institute of Radio Engineering and Electronics, Moscow 125009, Russia*

(Received 19 October 2015; revised manuscript received 1 February 2016; published 27 April 2016)

We use 2D coupled sine-Gordon equations combined with 3D heat diffusion equations to numerically investigate the thermal and electromagnetic properties of a $250 \times 70\ \mu m^2$ intrinsic Josephson junction stack. The 700 junctions are grouped to 20 segments; we assume that in a segment all junctions behave identically. At large input power, a hot spot forms in the stack. Resonant electromagnetic modes oscillating either along the length [(0, n) modes] or the width [(m, 0) modes] of the stack or having a more complex structure can be excited both with and without a hot spot. At fixed bath temperature and bias current, several cavity modes can coexist in the absence of a magnetic field. The (1, 0) mode considered to be the most favorable mode for terahertz emission can be stabilized by applying a small magnetic field along the length of the stack. A strong field-induced enhancement of the emission power is also found in experiment for an applied field around 5.9 mT.

DOI: 10.1103/PhysRevApplied.5.044017

I. INTRODUCTION

Stacks of intrinsic Josephson junctions (IJJs) in the high-temperature superconductor $Bi_2Sr_2CaCu_2O_8$ (BSCCO) emit coherent radiation at terahertz frequencies [1]. The emitted frequency f_e follows the Josephson relation $f_e = V_J/\Phi_0$, where Φ_0 is the flux quantum ($\Phi_0^{-1} = 483.6$ GHz/mV), and V_J is the voltage across a single junction. In BSCCO, superconductivity is restricted to $d_s = 0.3$ nm thick CuO_2 sheets separated by barrier layers to form an $s = 1.5$ nm thick IJJ [2]. In Ref. [1], stacks of approximately 700 IJJs, with a length $L_s \sim 300\ \mu$m and a width W_s of some 10 μm have been realized as mesas on top of BSCCO single crystals. These mesas emitted radiation between 0.35 and 0.85 THz, with an integrated output power of approximately 1 μW. The emission frequency scaled as W_s^{-1}, indicating that cavity modes oscillating along the width of the stack are responsible for synchronization. Terahertz radiation from IJJ stacks became a hot topic both in experiment [3–35] and theory [36–66]; for a recent review, see Ref. [67].

IJJ stacks containing 500–2000 junctions have been patterned as mesas but also as bare IJJ stacks contacted by Au layers (GBG structures) [16,17,20,24] and as all-superconducting structures [11]. Emission frequencies range from 0.3 to 2.4 THz. For the best stacks, an emission power P_e in the range of tens of microwatts has been achieved [17,19,20,32,33], and arrays of mesas showed emission with P_e up to 0.61 mW [19]. The physics of the huge IJJ stacks is affected by Joule heating [1,3,5,6,8,13,18,22,26,30,49,52,54,55,63]. For sufficiently low-bias currents, the temperature rises only slightly to values above the bath temperature $T_{\rm bath}$, and the voltage V across the stack increases with increasing bias current I. With increasing I and input power, the current-voltage characteristics (IVCs) start to backbend, and, at some bias current in the backbending region, a hot spot forms in the stack [3,6,8,13,18,21–23,25,26,34,68], creating a region heated to temperatures above the critical temperature T_c. Similar effects also occur in other systems [69,70]. The terahertz emission properties of the IJJ stacks are affected by the hot spot. For example, it has been found that the linewidth of radiation is much narrower in the high-bias regime than at low bias [12,60]. Other properties such as the emission frequency seem to be basically independent of the hot-spot position, leading to some debate as to whether the hot spot is helpful for radiation or just coexists with the radiating regions [20,22,23]. In fact, recent results showed that there is a strong interaction [28]. Further, cooling has been improved by sandwiching the stacks between substrates with high thermal conductivity. In the first attempts, maximum emission frequencies near 1.05 THz were obtained [24,68]. This value was recently improved to 2.4 THz for disk-shaped stacks [33]. In terms of modeling, many calculations of electrodynamics have been based on a homogeneous temperature distribution, while calculations of the thermal properties were based on solving the heat diffusion equations in the absence of Josephson currents [49,52,54]. Some attempts have been made to combine both electrodynamics and thermodynamics, either by using arrays of pointlike IJJs [59,60,64] or by incorporating temperature-induced effects into an effective model describing the whole stack as a single "giant" junction [55,62,63]. Reference [66] modeled the combined thermal and electromagnetic properties of BSCCO stacks via one-dimensional coupled sine-Gordon equations for an $N = 700$ junction stack where the IJJs were grouped into M segments [66].

II. MODEL

The model introduced here extends the 2D approach of Ref. [66] to 3D, enabling us to model IJJ stacks realistically. We first give a brief outline of the features which go beyond Ref. [66]. We consider a mesa consisting of $N = 700$ IJJs; cf. Fig. 1(a). The mesa has a length $L_s = 250\ \mu$m along x and a width $W_s = 70\ \mu$m along y. It is covered by a gold layer and centered on a 30-μm-thick base crystal of length $L_b = 2L_s$ and width $W_b = 2W_s$. The base crystal is mounted by a 20-μm-thick glue layer to a sample holder kept at T_{bath}. A bias current I is injected via a bond wire into the Au layer and leaves the mesa into the base crystal. The model contains a variety of parameters (in-plane and out-of-plane resistivities, Josephson critical current density, Cooper pair density, thermal conductances, etc.) which depend on the temperature. We assume that these parameters are spatially constant for spatially *constant* T. For an inhomogeneous temperature distribution in the stack, they vary in space through their dependence on the local temperature $T(x,y,z)$, which is found by self-consistently solving the thermal equations (requiring Joule heat dissipation as an input from the electric circuit) and the electrical equations (requiring the temperature distribution in the mesa, as determined from the thermal circuit).

For the thermal description [cf. Fig. 1(b)], we assume that the mesa plus the contacting Au layer and the bond wire have a temperature $T_m(x,y)$ which is constant along z but can vary along x and y. The BSCCO base crystal is split into K segments, the kth segment being at a temperature $T_{b,k}(x,y)$. For this geometry, we solve the heat diffusion equation

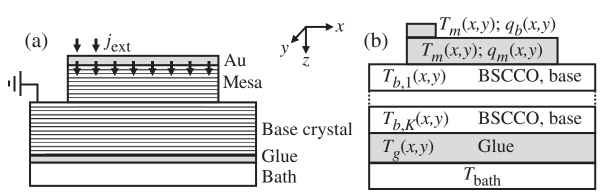

FIG. 1. Geometry used for modeling. Sketch of the mesa and electric current flow in the z direction (a). Geometry for thermal description (b), where q_m and q_b, respectively, denote the Joule power density produced in the mesa and by the bias lead. The temperatures of the various layers are indicated.

$$c\dot{T} = \nabla(\kappa\nabla T) + q_m + q_b, \tag{1}$$

with the specific heat capacity c, the (anisotropic) thermal conductivity κ, and the power densities q_m and q_b for heat generation in the mesa and the bond wire, respectively. For high enough q_b, the hot spot is controllably located near the wire position.

For the electric circuit, we group the N IJJs in the mesa to M segments, each containing $G = N/M$ IJJs, assumed to have identical properties. The bond wire injects an electric current density j_{ext} to the Au layer, which we assume to have a low enough resistance to freely distribute the current before it enters the IJJ stack in the z direction with a density $j_{z,\mathrm{Au}}$ proportional to the local BSCCO conductance $\sigma_c(x,y) = \rho_c^{-1}(x,y)$. The full expression is $j_{z,\mathrm{Au}} = \langle j_{\mathrm{ext}}\rangle \sigma_c(x,y)/\langle\sigma_c\rangle$, the brackets denoting spatial averaging. The interface stack-base crystal is treated as a ground. The z-axis currents consist of Josephson currents with critical current density $j_c(x,y)$, (Ohmic) quasiparticle currents with resistivity $\rho_c(x,y)$, and displacement currents with dielectric constant ε. To avoid weakly stable solutions, we also add Nyquist noise created by the quasiparticle currents. The in-plane currents consist of a superconducting part characterized by a Cooper pair density $n_s(x,y)$, a quasiparticle component with resistivity $\rho_{ab}(x,y)$, and a Nyquist noise component. For constant $T_m(x,y) = 4.2$ K, we index the above quantities by an additional "0" and assume that they are constant with respect to x and y. The temperature dependence of the various parameters is close to experimental curves and plotted in detail in Ref. [66]. We further use $T_c = 85$ K.

One obtains sine-Gordon-like equations for the Josephson phase differences $\gamma_m(x,y)$ in the mth segment of the IJJ stack:

$$\begin{aligned} &Gsd_s\nabla\left(\frac{\nabla\dot{\gamma}_m}{\rho_{ab}}\right) + d_s\nabla(j^N_{x,m+1} - j^N_{x,m}) + G\lambda_k^2\nabla(n_s\nabla\gamma_m) \\ &\quad = 2j_{z,m} - j_{z,m+1} - j_{z,m-1}. \end{aligned} \tag{2}$$

Here, $m = 1,\ldots,M$, $\nabla = (\partial/\partial x, \partial/\partial y)$, and $\lambda_k = [\Phi_0 d_s/(2\pi\mu_0 j_{c0}\lambda^2_{ab0})]^{1/2}$, with the in-plane London penetration depth λ_{ab0} and the magnetic permeability μ_0. Quantities $j^N_{x,m}$ are the in-plane noise current densities. Time is normalized to $\Phi_0/2\pi j_{c0}\rho_{c0}s$, resistivities to ρ_{c0}, and current densities to j_{c0}. Equation (2) neglects geometric inductances; i.e., it assumes that kinetic inductances dominate (valid if L_s, $W_s < \lambda_c$; $\lambda_c \sim 300\ \mu$m is the out-of-plane penetration depth).

For the out-of-plane current densities $j_{z,m}$, one finds

$$j_{z,m} = \beta_{c0}\ddot{\gamma}_m + \frac{\dot{\gamma}_m}{\rho_{c,m}} + j_c\sin(\gamma_m) + j^N_{z,m}, \tag{3}$$

with $\beta_{c0} = 2\pi j_{c0}\rho^2_{c0}\varepsilon\varepsilon_0 s/\Phi_0$; ε_0 is the vacuum permittivity, and the $j^N_{z,m}$ are the out-of-plane noise current densities.

From the gauge-invariant Josephson phase differences γ_m, as calculated from Eqs. (2) and (3), we obtain the phase ϕ_m of the superconducting wave function in electrodes m (the CuO_2 layer interfacing segments m and $m+1$) via

$$\nabla\gamma_m = \frac{2\pi s}{\Phi_0}(B_{y,m}, -B_{x,m}) + \frac{\nabla(\phi_{m+1} - \phi_m)}{G}. \quad (4)$$

Here, $B_{x,m}$ and $B_{y,m}$ are, respectively, the x and y components of the magnetic field in the mth segment.

The in-plane supercurrent densities in units of j_{c0}, $\vec{j}^s_m = (j^s_{x,m}, j^s_{y,m})$, in electrode m are expressed as

$$\vec{j}^s_m = \frac{\lambda_k^2 n_s}{d_s}\left(\nabla\phi_m - \frac{2\pi}{\Phi_0}\vec{A}_m\right). \quad (5)$$

$\vec{A}_m = (A_{x,m}, A_{y,m})$ denotes the in-plane components of the vector potential in electrode m. The resistive currents $\vec{j}^r_m = (j^r_{x,m}, j^r_{y,m})$ in electrode m are given by

$$\vec{j}^r_m = \frac{s}{\rho_{ab}}\frac{d}{dt}\left(\nabla\phi_m - \frac{2\pi}{\Phi_0}\vec{A}_m\right). \quad (6)$$

In our calculations, we assume that the z components of curl$\vec{j}^s_m$ and of curl$\vec{j}^r_m$ vanish, and, thus, inside the superconducting layers, the total magnetic field in the z direction is zero.

For the thermal parameters, we use the same values as in Ref. [66]. The bond wire with resistivity $\rho_b = 0.02\rho_{c0}$ is assumed to be a 25-μm-wide square located at the left edge of the mesa. Further, $\rho_{c0} = 10^3\ \Omega\,\mathrm{cm}$, $\rho_{ab0} = 8\ \mu\Omega\,\mathrm{cm}$, $j_{c0} = 200\ \mathrm{A/cm^2}$, $\lambda_{ab0} = 260$ nm, and $\varepsilon = 12$. For our geometry, one obtains a critical current $I_{c0} = 35$ mA, a c-axis resistance per junction $R_{c0} = 0.86\ \Omega$, a characteristic voltage $V_{c0} = I_{c0}R_{c0} = 30$ mV, and a characteristic frequency $f_{c0} = I_{c0}R_{c0}/\Phi_0 = 14.5$ THz. The characteristic power density $p_{c0} = j_{c0}^2\rho_{c0}$ is $4\times10^7\ \mathrm{W/cm^3}$, yielding for a stack volume of $1.84\times10^{-8}\ \mathrm{cm^3}$ a power P_{c0} of 0.74 W. For λ_k, one obtains 0.76 μm. The 4.2 K value of the in-phase mode velocity $c_1 = 8.8\times10^7$ m/s [66]. We keep the product $\beta_{c0}G$ constant in order to (approximately) fix the 4.2 K value of c_1 and use $\beta_{c0} = 4000$ for $G = 35$ ($M = 20$). We further divide ac electric fields and in-plane current densities by G to make the results only weakly dependent on M. For selected bias conditions, the scaling is tested using $M = 50$.

The differential equations are discretized using 50 (9) grid points along x (y) for the mesa and 100 (18) grid points for the base crystal [71], which is split into $K = 4$ segments. A fifth-order Runge-Kutta scheme is used to evolve these equations in time. After some initialization steps [66], various quantities partially averaged over spatial coordinates are tracked as a function of time to produce time averages or to make Fourier transforms.

III. RESULTS

Figure 2 shows for $T_{\mathrm{bath}} = 20$ K the averaged distributions of the power density $\langle q_\parallel(x,y)\rangle$ dissipated by in-plane currents for five values of $I/I_{c0} = 0.65$ Fig. 2(a) to 0.1 Fig. 2(e). Averaging is over time and the z direction in the mesa. This type of plot, also used in Ref. [66], is useful to visualize resonance patterns, with nodes (antinodes) appearing at the minima (maxima) of $\langle q_\parallel(x,y)\rangle$ [72]. The left (right) graphs are at high (low) bias where a hot spot is present (absent). In Figs. 2(a) and 2(e), the modulations along x are due to a cavity mode oscillating along x [a $(0,n)$ mode], with $n = 2$ and 3, respectively. In Fig. 2(c), a cavity mode oscillating along y is excited [a (1,0) mode]. The spatial variations in Figs. 2(b) and 2(d) have a more complicated structure which is not easy to explain by a superposition of different cavity modes. The patterns also show that "linear thinking" in terms of separating ac Josephson currents and resonant modes can be dangerous. Near the antinodes of the standing waves, vortex-antivortex pairs oscillate back and forth, colliding at the center of the antinode [66]. The collision zones should form a continuous line leaving the stack either at its edges or into the hot-spot area. All patterns fulfill this requirement.

In general, not all segments in the stack are synchronized. We investigate this by monitoring the dc voltages ($\propto$ Josephson oscillation frequency f_J) v_m ($m = 1,\ldots,M$) across the individual segments. For example, for the modes of Figs. 2(a)–2(c), for the two to three uppermost segments, v_m is about 1% higher than for the other (locked) segments. For the mode of Fig. 2(d), only small groups of two to five adjacent segments are locked. For the mode of Fig. 2(e), two groups of segments (one to seven and 10–20) oscillated at slightly different frequencies.

Note that $\langle q_\parallel(x,y)\rangle$ can have similar values for the $(0,n)$ and (1,0) modes; compare, e.g., Figs. 2(a) and 2(c). We expect that both types of modes radiate. However, for comparable values of $\langle q_\parallel(x,y)\rangle$, the *emission* power of the $(0,n)$ modes, with $n > 1$, will be lower, because the contributions of the oscillating (in-plane) currents to the magnetic vector potential partially cancel each other.

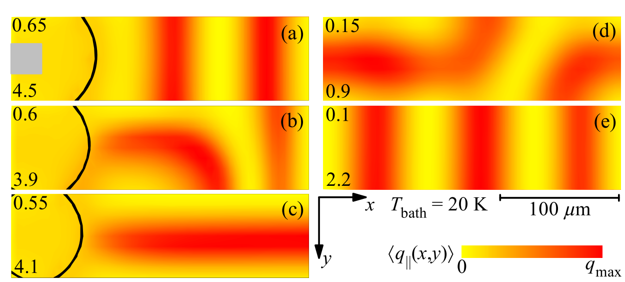

FIG. 2. Power density $\langle q_\parallel(x,y)\rangle$ in units of $10^{-5}\times j_{c0}^2\rho_{c0}$ (color scale) for five values of normalized bias current I/I_{c0} (upper left numbers); values for q_{max} at the bottom left. The gray square in (a) indicates the position of the bond wire. Regions enclosed by the black line are at $T_m \geq T_c$.

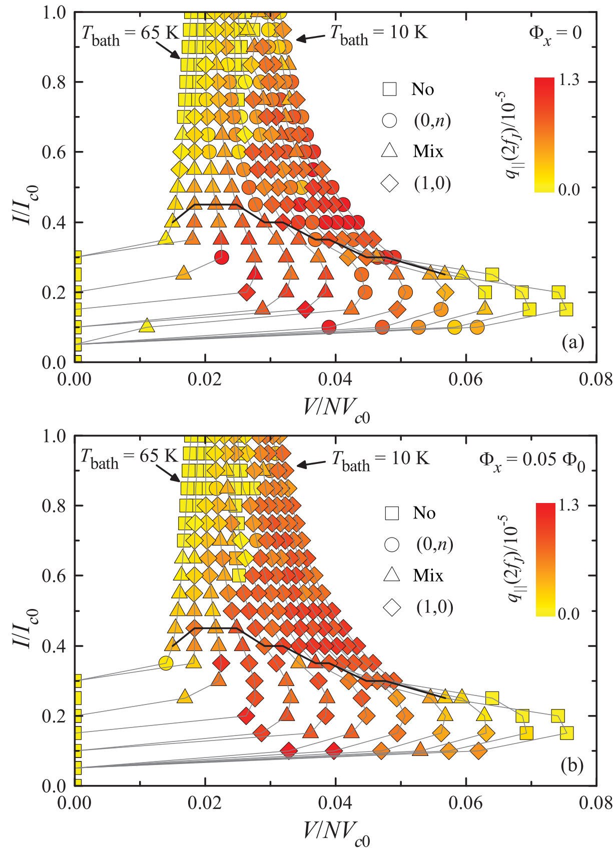

FIG. 3. Power density $q_{\|}(2f_J)$ in units of $10^{-5} \times j_{c0}^2 \rho_{c0}$ (color scale) vs normalized bias current and voltage across the stack for an applied magnetic field along x of (a) 0 and (b) 1 mT (0.05 Φ_0 per junction), applied along x. T_{bath} is varied from 10 to 65 K in steps of 5 K. $(0, n)$ modes, (1,0) modes, mixed resonances, and nonresonant states are marked by, respectively, circles, diamonds, triangles, and squares. The gray lines indicate IVCs at fixed T_{bath}. For data points at or above the black line (T_c line) a hot spot forms in the stack.

For the (1,0) mode, the in-plane currents at a given time have the same sign everywhere in the stack.

Figure 3(a) shows, for zero applied magnetic field, how different modes in the stack evolve as a function of I and T_{bath}. We record 12 IVCs for T_{bath} between 10 and 65 K. For each value of I and T_{bath}, we evaluate the type of mode by inspecting the plots as in Fig. 2 and encode it as the shape of the symbol in Fig. 3(a). To have a measure of the strength of a given mode, we record time traces $q_{\|}(t)$ of the power generated by in-plane currents, averaged over the stack volume. After Fourier transform, we extract from $q_{\|}(f)$ the power density $q_{\|}(2f_J)$ arising from the Josephson oscillations appearing as a peak at twice the Josephson frequency f_J. This quantity is plotted as the color scale for each data point. In Fig. 3(a), there are three regions where $q_{\|}(2f_J)$ is low: (i) for $I/I_{c0} > 0.5$ and $T_{bath} > 55$ K, (ii) for T_{bath} around 35 K and $I/I_{c0} > 0.65$, and (iii) for $V/NV_{c0} > 0.06$. In region (i), no or only a small fraction of the stack is superconducting; Josephson oscillations are absent or restricted to a small area. In region (ii) the in-plane and out-of-plane currents exhibit short-wavelength oscillations along x and y, indicative of a mode with spatial variations shorter than our grid spacing. The spectrum of $q_{\|}(f)$ is broad, with no significant peaks. In region (iii), where V and f_J are highest, all currents and fields vary smoothly, but no resonance is excited. In the presence of a hot spot [data points at or above the black line in Fig. 3(a)], $q_{\|}(2f_J)$ is large in a ribbon between $V/NV_{c0} \sim 0.025$ and 0.05. This regime extends down to approximately 0.02 in the low-bias regime. The relative broadness of this regime may look surprising, since resonant modes are excited; however, it can be understood from the facts that the mode velocities depend on the temperature [66] and vary significantly over the data points in Fig. 3(a). Also, the quality factor of the cavity modes is low (of order 10) at elevated temperatures. Most important, one notes that $(0, n)$, (1,0), and mixed modes vary almost randomly. Further simulations reveal that even for the same value of I and T_{bath}, different resonant modes can be excited. However, it should be possible to support the (1,0) mode favored for radiation by applying a small static magnetic field along x, imprinting a linear phase gradient and, consequently, a small gradient on the Josephson current along y. Figure 3(b) organized like Fig. 3(a) shows the resulting data for a small field B_x of 1 mT corresponding to a flux of $0.05\Phi_0$ per junction. The amplitudes of $q_{\|}(2f_J)$ are similar as in the zero-field case; however, the (1,0) mode has stabilized over a wide range of bias current and bath temperature.

IV. COMPARISON TO EXPERIMENT

We also test experimentally the potential benefit of a small magnetic field oriented along x, using a $75 \times 330\ \mu m^2$ large GBG structure with $N \approx 760$, mounted on a sapphire lens. Figure 4 shows for (a) $B_x = 0$ and (b) $B_x = 5.9$ mT ($0.32\Phi_0$ per junction) families of IVCs measured for 10 K $\leq T_{bath} \leq$ 45 K. IVCs at 0 and 5.9 mT are measured alternately at given T_{bath}. The accuracy in aligning the field with respect to out-of-plane tilts is better than 0.5°, and with respect to in-plane tilts, it is about 2°. The simultaneously detected terahertz emission power P_e measured via a Ge bolometer is plotted as a color scale. In the high-bias regime, the maximum emission power $P_{e,max}$ is 27.5 μW, while at low bias, it is 0.21 μW. We, thus, use different values for $P_{e,max}$ for $I > 8$ mA and for $I < 8$ mA; for fixed I, $P_{e,max}$ is the same in Figs. 4(a) and 4(b). For $B_x = 0$, the emission is strong for I between 10 and 20 mA and T_{bath} between 10 and 40 K. One notes short-period oscillations in P_e which presumably are extrinsic in origin. These oscillations have been observed before [28,35,66]. Apart from that, the plots clearly show that for $B_x = 5.9$ mT, over a wide range of currents and bath temperatures, P_e increases significantly in some of the stripelike regions up to a factor of 2.7. In the low-bias

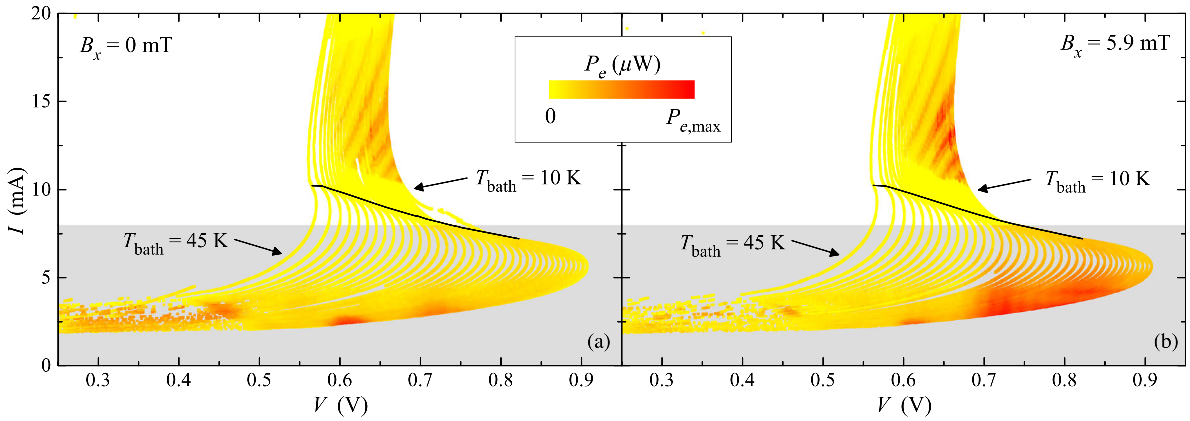

FIG. 4. Experimental data for a GBG structure: terahertz emission power P_e (color scale) for a large number of IVCs, measured at bath temperatures between 10 and 45 K for (a) $B_x = 0$ and (b) $B_x = 5.9$ mT. In both (a) and (b) $P_{e,\max} = 27.5$ μW for $I > 8$ mA and $P_{e,\max} = 0.21$ μW for $I < 8$ mA. Black lines in (a) and (b) indicate the T_c line.

regime, the effect is seen even more drastically, although on a much lower level of $P_{e,\max}$. The idea of applying a small field parallel to the long side of the stack, as suggested by the simulations, thus, seems to work. For other field orientations, the effect is not observed. Even a small field component perpendicular to the layers strongly suppresses P_e [73]. For the measurements shown above for out-of-plane tilts larger than about 1° (the precise value depends on bias current and bath temperature), the enhancement in emission power is lost in the high-bias regime. At the low-bias regime, the critical tilts are on the order of 3°–5°. Further, our simulations suggest that a field applied parallel to the short side is not helpful because a $(0, n)$ mode with $n > 1$ is not promoted by an applied flux well below $\Phi_0/2$ per junction. In Ref. [73], a 20% increase of P_e is observed for fields oriented in the a-b plane. Unfortunately, the field direction relative to the mesa edges is not reported.

V. SUMMARY

In summary, we present 3D simulations of the thermal and electromagnetic properties of a mesa consisting of 700 intrinsic junctions. Resonant modes can be excited in the stack both in the presence and in the absence of a hot spot, exhibiting standing waves either along the length [$(0, n)$ modes] or the width [(1,0) mode] of the stack. Also, more complex mixed modes are found. At fixed bath temperature and bias current, different modes can coexist. By applying a small magnetic field along the length of the stack, it is possible to stabilize the (1,0) mode considered to be the best mode for terahertz emission. In experiment, we find a strong field-induced enhancement of the emission power for a stand-alone stack for fields of around 5.9 mT, small enough to be created by a simple electromagnet.

ACKNOWLEDGMENTS

We gratefully acknowledge financial support by the National Natural Science Foundation of China (Grants No. 11234006 and No. 61501220), the Priority Academic Program Development of Jiangsu Higher Education Institutions, Jiangsu Provincial Natural Science Fund (Grant No. BK20150561), the Deutsche Forschungsgemeinschaft (Project No. KL930/13-1), JSPS KAKENHI Grant No. 25289108, Ministry of Education and Science of the Russian Federation (Grant No. 14.613.21.0046; ID RFMEFI61315X0046), and the EU-FP6-COST Action MP1201.

[1] L. Ozyuzer, A. E. Koshelev, C. Kurter, N. Gopalsami, Q. Li, M. Tachiki, K. Kadowaki, T. Yamamoto, H. Minami, H. Yamaguchi, T. Tachiki, K. E. Gray, W.-K. Kwok, and U. Welp, Emission of coherent THz radiation from superconductors, Science **318**, 1291 (2007).
[2] R. Kleiner, F. Steinmeyer, G. Kunkel, and P. Müller, Intrinsic Josephson Effects in $Bi_2Sr_2CaCu_2O_8$ Single Crystals, Phys. Rev. Lett. **68**, 2394 (1992).
[3] H. B. Wang, S. Guénon, J. Yuan, A. Iishi, S. Arisawa, T. Hatano, T. Yamashita, D. Koelle, and R. Kleiner, Hot Spots and Waves in $Bi_2Sr_2CaCu_2O_8$ Intrinsic Josephson Junction Stacks: A Study by Low Temperature Scanning Laser Microscopy, Phys. Rev. Lett. **102**, 017006 (2009).
[4] H. Minami, I. Kakeya, H. Yamaguchi, T. Yamamoto, and K. Kadowaki, Characteristics of terahertz radiation emitted from the intrinsic Josephson junctions in high-T_c superconductor $Bi_2Sr_2CaCu_2O_{8+\delta}$, Appl. Phys. Lett. **95**, 232511 (2009).
[5] C. Kurter, K. E. Gray, J. F. Zasadzinski, L. Ozyuzer, A. E. Koshelev, Q. Li, T. Yamamoto, K. Kadowaki, W. K. Kwok, M. Tachiki, and U. Welp, Thermal management in large Bi2212 mesas used for terahertz sources, IEEE Trans. Appl. Supercond. **19**, 428 (2009).
[6] S. Guénon, M. Grünzweig, B. Gross, J. Yuan, Z. G. Jiang, Y. Y. Zhong, M. Y. Li, A. Iishi, P. H. Wu, T. Hatano, R. G. Mints, E. Goldobin, D. Koelle, H. B. Wang, and R. Kleiner, Interaction of hot spots and THz waves in $Bi_2Sr_2CaCu_2O_8$

intrinsic Josephson junction stacks of various geometry, Phys. Rev. B **82**, 214506 (2010).

[7] C. Kurter, L. Ozyuzer, T. Proslier, J. F. Zasadzinski, D. G. Hinks, and K. E. Gray, Counterintuitive consequence of heating in strongly-driven intrinsic junctions of $Bi_2Sr_2CaCu_2O_{8+\delta}$ mesas, Phys. Rev. B **81**, 224518 (2010).

[8] H. B. Wang, S. Guénon, B. Gross, J. Yuan, Z. G. Jiang, Y. Y. Zhong, M. Grünzweig, A. Iishi, P. H. Wu, T. Hatano, D. Koelle, and R. Kleiner, Coherent Terahertz Emission of Intrinsic Josephson Junction Stacks in the Hot Spot Regime, Phys. Rev. Lett. **105**, 057002 (2010).

[9] M. Tsujimoto, K. Yamaki, K. Deguchi, T. Yamamoto, T. Kashiwagi, H. Minami, M. Tachiki, K. Kadowaki, and R. A. Klemm, Geometrical Resonance Conditions for THz Radiation from the Intrinsic Josephson Junctions in $Bi_2Sr_2CaCu_2O_{8+\delta}$, Phys. Rev. Lett. **105**, 037005 (2010).

[10] T. M. Benseman, A. E. Koshelev, K. E. Gray, W.-K. Kwok, U. Welp, K. Kadowaki, M. Tachiki, and T. Yamamoto, Tunable terahertz emission from $Bi_2Sr_2CaCu_2O_{8+\delta}$ mesa devices, Phys. Rev. B **84**, 064523 (2011).

[11] J. Yuan, M. Y. Li, J. Li, B. Gross, A. Ishii, K. Yamaura, T. Hatano, K. Hirata, E. Takayama Muromachi, P. H. Wu, D. Koelle, R. Kleiner, and H. B. Wang, Terahertz emission from $Bi_2Sr_2CaCu_2O_{8+\delta}$ intrinsic Josephson junction stacks with all-superconducting electrodes, Supercond. Sci. Technol. **25**, 075015 (2012).

[12] M. Y. Li, J. Yuan, N. Kinev, J. Li, B. Gross, S. Guénon, A. Ishii, K. Hirata, T. Hatano, D. Koelle, R. Kleiner, V. P. Koshelets, H. B. Wang, and P. H. Wu, Linewidth dependence of coherent terahertz emission from $Bi_2Sr_2CaCu_2O_8$ intrinsic Josephson junction stacks in the hot-spot regime, Phys. Rev. B **86**, 060505 (2012).

[13] I. Kakeya, Y. Omukai, T. Yamamoto, K. Kadowaki, and M. Suzuki, Effect of thermal inhomogeneity for terahertz radiation from intrinsic Josephson junction stacks of $Bi_2Sr_2CaCu_2O_{8+\delta}$, Appl. Phys. Lett. **100**, 242603 (2012).

[14] M. Tsujimoto, H. Minami, K. Delfanazari, M. Sawamura, R. Nakayama, T. Kitamura, T. Yamamoto, T. Kashiwagi, T. Hattori, and K. Kadowaki, Terahertz imaging system using high-T_c superconducting oscillation devices, J. Appl. Phys. **111**, 123111 (2012).

[15] M. Tsujimoto, T. Yamamoto, K. Delfanazari, R. Nakayama, T. Kitamura, M. Sawamura, T. Kashiwagi, H. Minami, M. Tachiki, K. Kadowaki, and R. A. Klemm, Broadly Tunable Subterahertz Emission from Internal Branches of the Current-Voltage Characteristics of Superconducting $Bi_2Sr_2CaCu_2O_{8+\delta}$ Single Crystals, Phys. Rev. Lett. **108**, 107006 (2012).

[16] T. Kashiwagi, M. Tsujimoto, T. Yamamoto, H. Minami, K. Yamaki, K. Delfanzari, K. Deguchi, N. Orita, T. Koike, R. Nakayama, T. Kitamura, M. Sawamura, S. Hagino, K. Ishida, K. Ivancovic, H. Asai, M. Tachiki, R. A. Klemm, and K. Kadowaki, High temperature superconductor terahertz emitters: Fundamental physics and its applications, Jpn. J. Appl. Phys. **51**, 010113 (2012).

[17] D. Y. An *et al.*, Terahertz emission and detection both based on high-T_c superconductors: Towards an integrated receiver, Appl. Phys. Lett. **102**, 092601 (2013).

[18] T. M. Benseman, A. E. Koshelev, W.-K. Kwok, U. Welp, V. K. Vlasko Vlasov, K. Kadowaki, H. Minami, and C. Watanabe, Direct imaging of hot spots in $Bi_2Sr_2CaCu_2O_{8+\delta}$ mesa terahertz sources, J. Appl. Phys. **113**, 133902 (2013).

[19] T. M. Benseman, K. E. Gray, A. E. Koshelev, W.-K. Kwok, U. Welp, H. Minami, K. Kadowaki, and T. Yamamoto, Powerful terahertz emission from $Bi_2Sr_2CaCu_2O_{8+\delta}$ mesa arrays, Appl. Phys. Lett. **103**, 022602 (2013).

[20] S. Sekimoto, C. Watanabe, H. Minami, T. Yamamoto, T. Kashiwagi, R. A. Klemm, and K. Kadowaki, Continuous 30 μW terahertz source by a high-T_c superconductor mesa structure, Appl. Phys. Lett. **103**, 182601 (2013).

[21] F. Turkoglu, L. Ozyuzer, H. Koseoglu, Y. Demirhan, S. Preu, S. Malzer, Y. Simsek, H. B. Wang, and P. Müller, Emission of the THz waves from large area mesas of superconducting $Bi_2Sr_2CaCu_2O_8$ by the injection of spin polarized current, Physica (Amsterdam) **491C**, 7 (2013).

[22] H. Minami, C. Watanabe, K. Sato, S. Sekimoto, T. Yamamoto, T. Kashiwagi, R. A. Klemm, and K. Kadowaki, Local SiC photoluminescence evidence of hot spot formation and sub-THz coherent emission from a rectangular $Bi_2Sr_2CaCu_2O_{8+\delta}$ mesa, Phys. Rev. B **89**, 054503 (2014).

[23] C. Watanabe, H. Minami, T. Yamamoto, T. Kashiwagi, R. A. Klemm, and K. Kadowaki, Spectral investigation of hot spot and cavity resonance effects on the terahertz radiation from high-T_c superconducting $Bi_2Sr_2CaCu_2O_{8+\delta}$ mesas, J. Phys. Condens. Matter **26**, 172201 (2014).

[24] M. Ji, J. Yuan, B. Gross, F. Rudau, D. Y. An, M. Y. Li, X. J. Zhou, Y. Huang, H. C. Sun, Q. Zhu, J. Li, N. Kinev, T. Hatano, V. P. Koshelets, D. Koelle, R. Kleiner, W. W. Xu, B. B. Jin, H. B. Wang, and P. H. Wu, $Bi_2Sr_2CaCu_2O_8$ intrinsic Josephson junction stacks with improved cooling: Coherent emission above 1 THz, Appl. Phys. Lett. **105**, 122602 (2014).

[25] M. Tsujimoto, H. Kambara, Y. Maeda, Y. Yoshioka, Y. Nakagawa, and I. Kakeya, Dynamic Control of Temperature Distributions in Stacks of Intrinsic Josephson Junctions in $Bi_2Sr_2CaCu_2O_{8+\delta}$ for Intense Terahertz Radiation, Phys. Rev. Applied **2**, 044016 (2014).

[26] C. Watanabe, H. Minami, T. Kitamura, K. Asanuma, K. Nakade, T. Yasui, Y. Saiwai, Y. Shibano, T. Yamamoto, T. Kashiwagi, R. A. Klemm, and K. Kadowaki, Influence of the local heating position on the terahertz emission power from high-T_c superconducting $Bi_2Sr_2CaCu_2O_{8+\delta}$ mesas, Appl. Phys. Lett. **106**, 042603 (2015).

[27] X. J. Zhou, J. Yuan, H. Wu, Z. S. Gao, M. Ji, D. Y. An, Y. Huang, F. Rudau, R. Wieland, B. Gross, N. Kinev, J. Li, A. Ishii, T. Hatano, V. P. Koshelets, D. Koelle, R. Kleiner, H. B. Wang, and P. H. Wu, Tuning the Terahertz Emission Power of an Intrinsic Josephson-Junction Stack with a Focused Laser Beam, Phys. Rev. Applied **3**, 044012 (2015).

[28] X. J. Zhou, Q. Zhu, M. Ji, D. Y. An, L. Y. Hao, H. Sun, S. Ishida, F. Rudau, R. Wieland, J. Li, D. Koelle, H. Eisaki, Y. Yoshida, T. Hatano, R. Kleiner, H. B. Wang, and P. H. Wu, Three-terminal stand-alone superconducting terahertz emitter, Appl. Phys. Lett. **107**, 122602 (2015).

[29] L. Y. Hao *et al.*, Compact Superconducting Terahertz Source Operating in Liquid Nitrogen, Phys. Rev. Applied **3**, 024006 (2015).

[30] B. Gross, F. Rudau, N. Kinev, M. Tsujimoto, J. Yuan, Y. Huang, M. Ji, X. J. Zhou, D. Y. An, A. Ishii, P. H. Wu, T. Hatano, D. Koelle, H. B. Wang, V. P. Koshelets, and R.

Kleiner, Electrothermal behavior and terahertz emission properties of a planar array of two $Bi_2Sr_2CaCu_2O_{8+\delta}$ intrinsic Josephson junction stacks, Supercond. Sci. Technol. **28**, 055004 (2015).
[31] I. Kakeya, N Hirayama, Y. Omukai, and M. Suzuki, Temperature dependence of terahertz emission by an asymmetric intrinsic Josephson junction device, J. Appl. Phys. **117**, 043914 (2015).
[32] T. Kashiwagi, T. Yamamoto, T. Kitamura, K. Asanuma, C. Watanabe, K. Nakade, T. Yasui, Y. Saiwai, Y. Shibano, H. Kubo, K. Sakamoto, T. Katsuragawa, M. Tsujimoto, K. Delfanazari, R. Yoshizaki, H. Minami, R. A. Klemm, and K. Kadowaki, Generation of electromagnetic waves from 0.3 to 1.6 terahertz with a high-T_c superconducting $Bi_2Sr_2CaCu_2O_{8+\delta}$ intrinsic Josephson junction emitter, Appl. Phys. Lett. **106**, 092601 (2015).
[33] T. Kashiwagi, K. Sakamoto, H. Kubo, Y. Shibano, T. Enomoto, T. Kitamura, K. Asanuma, T. Yasui, C. Watanabe, K. Nakade, Y. Saiwai, T. Katsuragawa, M. Tsujimoto, R. Yoshizaki, T. Yamamoto, H. Minami, R. A. Klemm, and K. Kadowaki, A high-T_c intrinsic Josephson junction emitter tunable from 0.5 to 2.4 terahertz, Appl. Phys. Lett. **107**, 082601 (2015).
[34] T. M. Benseman, A. E. Koshelev, V. Vlasko-Vlasov, Y. Hao, W.-K. Kwok, U. Welp, C. Keiser, B. Gross, M. Lange, D. Kölle, R. Kleiner, H. Minami, C. Watanabe, and K. Kadowaki, Current Filamentation in Large $Bi_2Sr_2CaCu_2O_{8+\delta}$ Mesa Devices Observed via Luminescent and Scanning Laser Thermal Microscopy, Phys. Rev. Applied **3**, 044017 (2015).
[35] M. Tsujimoto, I. Kakeya, T. Kashiwagi, H. Minami, and K. Kadowaki, Cavity mode identification for coherent terahertz emission from high-T_c superconductors, Opt. Express **24**, 4591 (2016).
[36] L. N. Bulaevskii and A. E. Koshelev, Radiation Due to Josephson Oscillations in Layered Superconductors, Phys. Rev. Lett. **99**, 057002 (2007).
[37] A. E Koshelev and L. N. Bulaevskii, Resonant electromagnetic emission from intrinsic Josephson-junction stacks with laterally modulated Josephson critical current, Phys. Rev. B **77**, 014530 (2008).
[38] S. Z. Lin and X. Hu, Possible Dynamic States in Inductively Coupled Intrinsic Josephson Junctions of Layered High-T_c Superconductors, Phys. Rev. Lett. **100**, 247006 (2008).
[39] V. M. Krasnov, Nonlinear Nonequilibrium Quasiparticle Relaxation in Josephson Junctions, Phys. Rev. Lett. **103**, 227002 (2009).
[40] R. A. Klemm and K. Kadowaki, Output from a Josephson stimulated terahertz amplified radiation emitter, J. Phys. Condens. Matter **22**, 375701 (2010).
[41] M. Tachiki, S. Fukuya, and T. Koyama, Mechanism of Terahertz Electromagnetic Wave Emission from Intrinsic Josephson Junctions, Phys. Rev. Lett. **102**, 127002 (2009).
[42] N. F. Pedersen and S. Madsen, THz generation using fluxon dynamics in high temperature superconductors, IEEE Trans. Appl. Supercond. **19**, 726 (2009).
[43] X. Hu and S. Z. Lin, Cavity phenomena in mesas of cuprate high-T_c superconductors under voltage bias, Phys. Rev. B **80**, 064516 (2009).
[44] T. Koyama, H. Matsumoto, M. Machida, and K. Kadowaki, In-phase electrodynamics and terahertz wave emission in extended intrinsic Josephson junctions, Phys. Rev. B **79**, 104522 (2009).
[45] V. M. Krasnov, Coherent flux-flow emission from stacked Josephson junctions: Nonlocal radiative boundary conditions and the role of geometrical resonances, Phys. Rev. B **82**, 134524 (2010).
[46] A. E. Koshelev, Stability of dynamic coherent states in intrinsic Josephson-junction stacks near internal cavity resonance, Phys. Rev. B **82**, 174512 (2010).
[47] S. Z. Lin and X. Hu, Response and amplification of terahertz electromagnetic waves in intrinsic Josephson junctions of layered high-T_c superconductor, Phys. Rev. B **82**, 020504 (2010).
[48] S. O. Katterwe, A. Rydh, H. Motzkau, A. B. Kulakov, and V. M. Krasnov, Superluminal geometrical resonances observed in $Bi_2Sr_2CaCu_2O_{8+x}$ intrinsic Josephson junctions, Phys. Rev. B **82**, 024517 (2010).
[49] A. A. Yurgens, Temperature distribution in a large $Bi_2Sr_2CaCu_2O_{8+\delta}$ mesa, Phys. Rev. B **83**, 184501 (2011).
[50] T. Koyama, H. Matsumoto, M. Machida, and Y. Ota, Multiscale simulation for terahertz wave emission from the intrinsic Josephson junctions, Supercond. Sci. Technol. **24**, 085007 (2011).
[51] V. M. Krasnov, Terahertz electromagnetic radiation from intrinsic Josephson junctions at zero magnetic field via breather-type self-oscillations, Phys. Rev. B **83**, 174517 (2011).
[52] A. Yurgens and L. N. Bulaevskii, Temperature distribution in a stack of intrinsic Josephson junctions with their CuO-plane electrodes oriented perpendicular to supporting substrate, Supercond. Sci. Technol. **24**, 015003 (2011).
[53] S. Z. Lin, X. Hu, and L. N. Bulaevskii, Synchronization in a one-dimensional array of point Josephson junctions coupled to a common load, Phys. Rev. B **84**, 104501 (2011).
[54] B. Gross, S. Guénon, J. Yuan, M. Y. Li, J. Li, A. Ishii, R. G. Mints, T. Hatano, P. H. Wu, D. Koelle, H. B. Wang, and R. Kleiner, Hot-spot formation in stacks of intrinsic Josephson junctions in $Bi_2Sr_2CaCu_2O_8$, Phys. Rev. B **86**, 094524 (2012).
[55] H. Asai, M. Tachiki, and K. Kadowaki, Three-dimensional numerical analysis of terahertz radiation emitted from intrinsic Josephson junctions with hot spots, Phys. Rev. B **85**, 064521 (2012).
[56] H. Asai, M. Tachiki, and K. Kadowaki, Proposal of terahertz patch antenna fed by intrinsic Josephson junctions, Appl. Phys. Lett. **101**, 112602 (2012).
[57] Y. X. Zhang, Y. C. Zhou, L. Dong, and S. G. Liu, Coherent terahertz radiation from high-harmonic component of modulated free-electron beam in a tapered two-asymmetric grating structure, Appl. Phys. Lett. **101**, 123503 (2012).
[58] S. Z. Lin and X. Hu, In-plane dissipation as a possible synchronization mechanism for terahertz radiation from intrinsic Josephson junctions of layered superconductors, Phys. Rev. B **86**, 054506 (2012).
[59] A. Grib and P. Seidel, The influence of standing waves on synchronization and self-heating of Josephson junctions in resonant systems, Low Temp. Phys. **38**, 321 (2012).

[60] B. Gross, J. Yuan, D. Y. An, M. Y. Li, N. Kinev, X. J. Zhou, M. Ji, Y. Huang, T. Hatano, R. G. Mints, V. P. Koshelets, P. H. Wu, H. B. Wang, D. Koelle, and R. Kleiner, Modeling the linewidth dependence of coherent terahertz emission from intrinsic Josephson junction stacks in the hot-spot regime, Phys. Rev. B **88**, 014524 (2013).

[61] F. Liu, S. Z. Lin, and X. Hu, Cavity phenomenon and terahertz radiation of a tall stack of intrinsic Josephson junctions wrapped by a dielectric material, Supercond. Sci. Technol. **26**, 025003 (2013).

[62] H. Asai and S. Kawabata, An effect of temperature distribution on terahertz phase dynamics in intrinsic Josephson junctions, Physica (Amsterdam) **494C**, 121 (2013).

[63] H. Asai and S. Kawabata, Intense terahertz emission from intrinsic Josephson junctions by external heat control, Appl. Phys. Lett. **104**, 112601 (2014).

[64] A. Grib and P. Seidel, The influence of external separate heating on the synchronization of Josephson junctions, Phys. Status Solidi (b) **251**, 1040 (2014).

[65] S. Z. Lin, Mutual synchronization of two stacks of intrinsic Josephson junctions in cuprate superconductors, J. Appl. Phys. **115**, 173901 (2014).

[66] F. Rudau, M. Tsujimoto, B. Gross, T. E. Judd, R. Wieland, E. Goldobin, N. Kinev, J. Yuan, Y. Huang, M. Ji, X. J. Zhou, D. Y. An, A. Ishii, R. G. Mints, P. H. Wu, T. Hatano, H. B. Wang, V. P. Koshelets, D. Koelle, and R. Kleiner, Thermal and electromagnetic properties of $Bi_2Sr_2CaCu_2O_8$ intrinsic Josephson junction stacks studied via one-dimensional coupled sine-Gordon equations, Phys. Rev. B **91**, 104513 (2015).

[67] U. Welp, K. Kadowaki, and R. Kleiner, Superconducting emitters of THz radiation, Nat. Photonics **7**, 702 (2013).

[68] T. Kitamura, T. Kashiwagi, T. Yamamoto, M. Tsujimoto, C. Watanabe, K. Ishida, S. Sekimoto, K. Asanuma, T. Yasui, K. Nakade, Y. Shibano, Y. Saiwai, H. Minami, R. A. Klemm, and K. Kadowaki, Broadly tunable, high-power terahertz radiation up to 73 K from a stand-alone $Bi_2Sr_2CaCu_2O_{8+\delta}$ mesa, Appl. Phys. Lett. **105**, 202603 (2014).

[69] A. Vl. Gurevich and R. G. Mints, Self-heating in normal metals and superconductors, Rev. Mod. Phys. **59**, 941 (1987).

[70] E. Spenke, Zur technischen Beherrschung des Wärmedurchschlages von Heissleitern, Wiss. Veröffentl. Siemens-Werken **15**, 92 (1936).

[71] Note that for $M = 20$ and the relatively low number of grid points along x and y, we cannot resolve modes that fluctuate strongly in space, like antiphase oscillations of different junctions or static triangular fluxon lattices appearing in magnetic fields on the order of a flux quantum per junction. However, we are mainly interested in dynamic in-phase solutions which can be captured well with the discretization used.

[72] A perhaps more natural choice is to look at the time average $\langle E_z^2(x,y)\rangle$ of the square of the z-axis electric fields. However, $E_z(x,y,z,t)$ has a large dc component, and features of oscillating standing waves are only weakly visible.

[73] K. Yamaki, M. Tsujimoto, T. Yamamoto, H. Minami, and K. Kadowaki, Magnetic field effects on THz radiation from rectangular shape Bi2212 IJJs, Physica (Amsterdam) **470C**, S804 (2010).